

Chiral Anomaly Induced Transverse Planar Transport Phenomena in Three Dimensional Spin-Orbit Coupled Metals

Rishi G. Gopalakrishnan,¹ Binayyak B. Roy,¹ Gargee Sharma,² and Sumanta Tewari¹

¹*Department of Physics and Astronomy, Clemson University, Clemson, SC 29634, USA*

²*Department of Physics, Indian Institute of Technology Delhi, Hauz Khas, New Delhi-110016, India*

We investigate linear and nonlinear transverse planar transport phenomena (viz. linear and nonlinear Hall and Nernst coefficients) induced by chiral anomaly in three-dimensional spin-orbit coupled metallic systems. Unlike Weyl semimetals, these systems do not possess multiple Weyl nodes located at isolated points in the momentum space but instead host a pair of Fermi surfaces characterized by opposite Berry curvature fluxes enclosing the same band-degeneracy point. Using semiclassical Boltzmann transport formalism within the relaxation time approximation, we derive first- and second-order transverse planar transport coefficients induced by electrical and thermal gradients in the presence of an in-plane magnetic field. Our analysis reveals distinctive angular dependencies of the transport coefficients, along with characteristic scaling behavior with the magnetic field strength. Furthermore, we demonstrate that the anomaly-induced transport coefficients exhibit an exponential temperature dependence. This unconventional behavior leads to the violations of the Mott relation at comparatively low temperatures, highlighting unique thermoelectric signatures that can be probed experimentally in 3D spin-orbit coupled metallic systems.

I. INTRODUCTION

Recent advancements in condensed matter physics have demonstrated that certain classes of materials, known as topological materials, can host exotic quasiparticles whose properties resemble those predicted in high-energy physics [1–3]. These systems are characterized by topologically protected band degeneracies and nontrivial electronic structures, giving rise to phenomena analogous to relativistic effects in particle physics. Examples include topological insulators, which possess gapless edge or surface states protected by time-reversal symmetry [1, 2]; Weyl semimetals, featuring pairs of topologically stable Weyl nodes that act as sources or sinks of Berry curvature in momentum space [3–14]; Dirac semimetals, characterized by fourfold degenerate nodes stabilized by symmetries like rotation or inversion [15–25]; and topological superconductors, promising candidates for realizing Majorana fermions with potential applications in fault-tolerant quantum computing [26–32].

The intriguing correspondence between high-energy and condensed matter physics has not only deepened our understanding of fundamental physics but has also opened pathways to realizing phenomena once thought exclusive to particle physics experiments [33–35]. For instance, phenomena such as the chiral anomaly—originally discussed in the context of quantum field theory [36, 37]—have now been realized experimentally in Weyl and Dirac semimetals [38–43]; such realizations allow condensed matter systems to serve as experimental platforms to probe quantum anomalies and their associated transport signatures [44–49]. Chiral anomaly refers to the non-conservation of chiral charge in the presence of parallel electric and magnetic fields ($\mathbf{E} \cdot \mathbf{B} \neq 0$). In Weyl semimetals, this leads to distinct experimental signatures such as negative longitudinal magnetoresistance and the planar Hall and Nernst effects [46, 50–87].

The presence of chiral anomaly in these materials can be intuitively understood in terms of the Berry curvature monopoles associated with Weyl nodes, acting effectively as sources and sinks of Berry flux in momentum space [3, 4]. While initially explored theoretically, these chiral-anomaly-induced transport effects have now been robustly confirmed experimentally [65, 88], highlighting their practical significance as probes of the fundamental topological character in semimetallic systems.

In this paper, we extend our analysis beyond Weyl semimetals to investigate anomaly-induced transport in three-dimensional metallic systems characterized by strong spin-orbit coupling (SOC) [89–93]. Unlike Weyl semimetals, these systems do not host pairs of separated Weyl nodes (see Fig. 2); instead, the system studied here features a single degeneracy point accompanied by distinct Fermi surfaces, each characterized by non-zero Berry curvature flux, while the net flux integrated over all Fermi surfaces vanishes, as expected from the Nielsen-Ninomiya theorem [94, 95]. Recently, it was demonstrated that such systems can support both the chiral anomaly and its thermal analog—the gravitational chiral anomaly—under parallel electric (or thermal gradient) and magnetic fields [89–92].

To derive the relevant transport properties, we employ the semiclassical Boltzmann transport formalism [96–99] and examine the behavior in the low-temperature limit at both linear and second order in electric field/ thermal gradient. Recent studies showed that chiral anomaly induced second-order transport coefficients, under the Sommerfeld expansion, obey the non-linear analogs of the Wiedemann-Franz Law and Mott relations [100, 101]. We will show in this paper, that such relations hold in our system at very low temperatures, but quickly break down as temperature is increased as polynomial approximations to the underlying energy integrals are rendered invalid. We will further investigate distinctive characteristics of these transport coefficients by examining

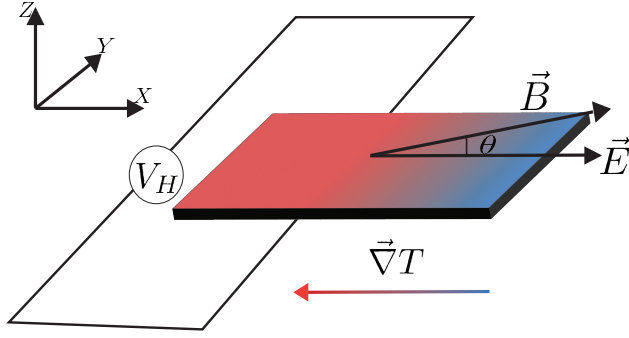


Figure 1. Schematic of experimental geometry to measure planar transverse response generated by an in-plane magnetic field (\mathbf{B}) in the presence of a thermal gradient (∇T) and/or an electric field (\mathbf{E}).

ing their dependence on the angle between the applied magnetic field and the electric field or thermal gradient. Specifically, we demonstrate that the extrema for these transport responses occur at distinct angular positions: at linear order, the transport coefficients peak at $\theta = \pi/4$, whereas at quadratic order, the extrema shift to $\theta = \arctan(1/\sqrt{2})$. Additionally, our analysis shows that the transport coefficients depend on the magnetic field strength, scaling quadratically ($\sim B^2$) at linear order and cubically ($\sim B^3$) at quadratic order in the electric field and/or the temperature gradient.

The paper is organized as follows: In Section II, we introduce and derive the semiclassical Boltzmann transport equations used in our analysis. In Section III, we employ these equations to demonstrate the emergence of the chiral anomaly and to derive both linear and non-linear anomaly-induced planar transverse transport coefficients. In Section IV we apply our theoretical framework to 3D spin-orbit coupled metallic systems, illustrating the presence of distinctive transport signatures of the chiral anomaly in such systems. Finally, in Section V, we summarize our key findings and provide concluding remarks. Additional details and calculations supporting our results are provided in the Appendix.

II. SEMICLASSICAL CHARGE TRANSPORT IN BOLTZMANN TRANSPORT EQUATIONS

In the presence of a non-zero Berry curvature as well as electric and magnetic fields, the semiclassical motion of Bloch electrons acquires anomalous terms. Their dy-

namics are described by the equations of motion [102]

$$\dot{\mathbf{r}}^s = D \left[\mathbf{v}^s + \frac{e}{\hbar} \mathbf{E} \times \boldsymbol{\Omega}^s + \frac{e}{\hbar} (\mathbf{v}^s \cdot \boldsymbol{\Omega}^s) \mathbf{B} \right], \quad (1)$$

$$\dot{\mathbf{k}}^s = D \left[-\frac{e}{\hbar} \mathbf{E} - \frac{e}{\hbar} \mathbf{v}^s \times \mathbf{B} + \frac{e^2}{\hbar^2} (\mathbf{E} \cdot \mathbf{B}) \boldsymbol{\Omega}^s \right], \quad (2)$$

where $\boldsymbol{\Omega}^s$ is the Berry curvature (with band/chirality index $s = \pm 1$) and $(D^s)^{-1} = 1 + \frac{e}{\hbar} (\mathbf{B} \cdot \boldsymbol{\Omega}^s)$ is the modified phase-space Jacobian, which reduces to unity when $\boldsymbol{\Omega}^s = 0$. The band velocity is $\mathbf{v}^s = (1/\hbar) \nabla_k \epsilon_k$. The second term in Eq. (1) is the anomalous Hall velocity, and the last term, proportional to $(\mathbf{v}^s \cdot \boldsymbol{\Omega}^s) \mathbf{B}$, is known as the *chiral magnetic velocity*. Although it can generate charge currents without external driving, such contributions cancel between opposite chiralities when no electric field or thermal gradient is applied, leaving the net equilibrium current zero.

When an external electric field or a temperature gradient is applied, the non-equilibrium distribution $f_k^s(\mathbf{r}, \mathbf{k}, t)$ evolves according to [85]

$$\begin{aligned} \left(\partial_t + \dot{\mathbf{r}} \cdot \nabla_{\mathbf{r}} + \dot{\mathbf{k}} \cdot \nabla_{\mathbf{k}} \right) f_k^s &= - \frac{f_k^s - f_{eq}(\epsilon^s, \mu^s, T^s)}{\tau_0} \\ &\quad - \frac{f_k^s - f_{eq}(\epsilon^s, \mu^{\bar{s}}, T^{\bar{s}})}{\tau_{\nu}}, \end{aligned} \quad (3)$$

where τ_0 and τ_{ν} are the intra- and inter-chiral center relaxation times. Including both scattering channels is essential for reaching a steady state when charge is pumped between the two chiral centers. In the relaxation-time picture, the first term drives the chiral carriers toward the local equilibrium of the *same* chiral center, while the second relaxes them toward the equilibrium distribution of the *opposite* center.

Substituting Eqs. (1) and (2) into the kinetic equation (3) and retaining only the term proportional to $(\mathbf{v}^s \cdot \boldsymbol{\Omega}^s) \mathbf{B}$ - the part responsible for the axial (chiral) anomaly - we obtain

$$\begin{aligned} D^s \left(\mathbf{v}^s + \frac{e}{\hbar} (\mathbf{v}^s \cdot \boldsymbol{\Omega}^s) \mathbf{B} \right) \cdot \left[e \mathbf{E} + \left(\frac{\epsilon^s - \mu}{T} \right) \nabla T \right] \left(-\frac{\partial f_k^s}{\partial \epsilon^s} \right) \\ = -\frac{\delta f_k^s}{\tau^*} - \frac{f_{eq}(\epsilon^s, \mu^s, T^s) - f_{eq}(\epsilon^s, \mu^{\bar{s}}, T^{\bar{s}})}{\tau_{\nu}}, \end{aligned} \quad (4)$$

where $\tau^{*-1} = \tau_0^{-1} + \tau_{\nu}^{-1}$. In deriving Eq. (4) we have omitted cross-product terms such as $\mathbf{E} \times \boldsymbol{\Omega}^s$ and $\mathbf{v}^s \times \mathbf{B}$ in Eqs. (1) and (2) respectively, because they do not contribute to chiral anomaly. As a consistency check, setting $\mathbf{E} = \nabla T = 0$ forces $\delta f_k^s \rightarrow 0$ since the chemical potential and temperature difference between the chiral centers vanishes in the absence of the chiral anomaly, thereby recovering the Fermi-Dirac equilibrium distribution $f_{eq} = 1/(e^{\beta(\epsilon_k - \mu)} + 1)$. Even in the absence of \mathbf{E} or ∇T , a uniform magnetic field drives an *equilibrium* current at each chiral center through the chiral magnetic velocity in Eq. (1):

$$j_{eq}^s = -e(\mu C_s^0 + k_B T C_s^1) \mathbf{B}, \quad (5)$$

where the Berry-flux moments C_s^ν are defined in Eq. (21). Because the two chiralities contribute equal and opposite values, the net equilibrium current cancels.

When there is a non-zero \mathbf{E} or (and) ∇T satisfying $\mathbf{E} \parallel \mathbf{B}$ or (and) $\nabla T \parallel \mathbf{B}$, the anomaly pumps charge and energy between the two chiral centers without changing the total carrier number. This is known as chiral anomaly [34–36]. In condensed matter systems, it leads to imbalances in the chemical potential (μ^s) and temperature (T^s) between the chiral centers. These imbalances scale linearly with $\mathbf{E} \cdot \mathbf{B}$ (chiral anomaly) and $\nabla T \cdot \mathbf{B}$ (gravitational anomaly). We denote the deviations from equilibrium chemical potential and temperature on the chiral center s by $\delta\tilde{\mu}^s$ and $\delta\tilde{T}^s$, respectively. We define the average deviation for each chiral center as

$$\delta\mu^s = \frac{\delta\tilde{\mu}^s - \delta\tilde{\mu}^{\bar{s}}}{2}, \quad \delta T^s = \frac{\delta\tilde{T}^s - \delta\tilde{T}^{\bar{s}}}{2}.$$

This formulation is convenient, as it ensures that the deviations in chemical potential and temperature for the two chiral centers are equal in magnitude and opposite in sign. To linear order in \mathbf{E} and ∇T , $\delta\mu^s$ and δT^s are determined using the transport equation (Eq. 4)

$$\begin{aligned} \delta\mu^s &= -\frac{\tau_\nu}{2} \left(\frac{\mathcal{D}_s^1 \mathcal{D}_s^2}{\mathcal{D}_s^0 \mathcal{D}_s^2 - (\mathcal{D}_s^1)^2} \right) \left[\left(\frac{\Lambda_s^0}{\mathcal{D}_s^1} - \frac{\Lambda_s^1}{\mathcal{D}_s^2} \right) \cdot e\mathbf{E} \right. \\ &\quad \left. + \left(\frac{\Lambda_s^1}{\mathcal{D}_s^1} - \frac{\Lambda_s^2}{\mathcal{D}_s^2} \right) \cdot \frac{\nabla T}{T} \right], \end{aligned} \quad (6)$$

$$\begin{aligned} \frac{\delta T^s}{T} &= -\frac{\tau_\nu}{2} \left(\frac{\mathcal{D}_s^0 \mathcal{D}_s^1}{\mathcal{D}_s^0 \mathcal{D}_s^2 - (\mathcal{D}_s^1)^2} \right) \left[\left(\frac{\Lambda_s^1}{\mathcal{D}_s^1} - \frac{\Lambda_s^2}{\mathcal{D}_s^2} \right) \cdot e\mathbf{E} \right. \\ &\quad \left. + \left(\frac{\Lambda_s^2}{\mathcal{D}_s^1} - \frac{\Lambda_s^0}{\mathcal{D}_s^0} \right) \cdot \frac{\nabla T}{T} \right] \end{aligned} \quad (7)$$

For more details, refer Appendix A. Here D_s^ν and Λ_s^ν are generalized density and energy–velocity moments:

$$\mathcal{D}_s^\nu = \int \frac{d^3k}{(2\pi)^3} (D^s)^{-1} \left(-\frac{\partial f_{eq}}{\partial \epsilon} \right) (\epsilon^s - \mu)^\nu, \quad (8)$$

$$\begin{aligned} \Lambda_s^\nu &= \int \frac{d^3k}{(2\pi)^3} \left(-\frac{\partial f_{eq}}{\partial \epsilon} \right) \left[\mathbf{v}^s + \frac{e}{\hbar} (\mathbf{v}^s \cdot \boldsymbol{\Omega}^s) \mathbf{B} \right] (\epsilon^s - \mu)^\nu \\ &= \int \frac{d^3k}{(2\pi)^3} \left(-\frac{\partial f_{eq}}{\partial \epsilon} \right) \frac{e}{\hbar} (\mathbf{v}^s \cdot \boldsymbol{\Omega}^s) \mathbf{B} (\epsilon^s - \mu)^\nu, \end{aligned} \quad (9)$$

The second line of Eq. (9) follows from the fact that the angular average of \mathbf{v}^s vanishes. To extract transport coefficients we expand the non-equilibrium distribution function in powers of the the electric field and thermal gradient,

$$\delta f_k^s \equiv f_k^s - f_{eq} = \sum_{n \geq 1} f_k^{(n)}, \quad (10)$$

where $f_k^{(n)}$ collects all terms of n th order in \mathbf{E} and ∇T , including every permutation. We work in the *chiral limit* [85], defined by $\tau_\nu \gg \tau_0 \simeq \tau^*$, which ensures that

the leading corrections to the transport coefficients arise solely from anomaly-induced charge pumping. Expanding the inter-chiral center collision term on the right-hand side of Eq. (4) to first and second order then yields

$$f_k^{(1)} = -2 \frac{\tau^*}{\tau_\nu} \frac{\partial f_{eq}}{\partial \epsilon^s} \left[\delta\mu^s + \frac{\epsilon^s - \mu}{T} \delta T^s \right], \quad (11)$$

$$\begin{aligned} f_k^{(2)} &= -2 \frac{\tau^*}{\tau_\nu} \left\{ (\delta\mu^s)^2 \frac{\partial^2 f_{eq}}{\partial \epsilon^{s2}} + \frac{2\delta\mu^s \delta T^s}{T} \left[\frac{\partial f_{eq}}{\partial \epsilon^s} + \right. \right. \\ &\quad \left. (\epsilon^s - \mu) \frac{\partial^2 f_{eq}}{\partial \epsilon^{s2}} \right] + \frac{(\delta T^s)^2}{T^2} \left[2(\epsilon^s - \mu) \frac{\partial f_{eq}}{\partial \epsilon^s} \right. \\ &\quad \left. \left. + (\epsilon^s - \mu)^2 \frac{\partial^2 f_{eq}}{\partial \epsilon^{s2}} \right] \right\}. \end{aligned} \quad (12)$$

A complete derivation is provided in Appendix A. We omit orbital magnetic-moment contributions, as they are negligible for chiral-anomaly-driven nonlinear responses [91, 103, 104]. The next section employs Eqs. (6)–(12) to obtain the linear and quadratic planar response coefficients.

III. CHIRAL ANOMALY INDUCED CHARGE TRANSPORT

We now derive the charge currents arising from each chiral center in the presence of an applied electric field and thermal gradient. Starting from the semiclassical equations of motion in the presence of Berry curvature, the charge current for carriers of chirality s is

$$\mathbf{j}_e^s = \int [dk] (D^s)^{-1} \dot{\mathbf{r}} \delta f_k^s, \quad (13)$$

where $[dk] \equiv d^3k/(2\pi)^3$. Employing Eq. (10) we rewrite this as

$$\begin{aligned} \mathbf{j}_e^s &= \int [dk] (D^s)^{-1} \dot{\mathbf{r}} (f_k^s - f_{eq}^s) \\ &= \int [dk] \sum_n (D^s)^{-1} \dot{\mathbf{r}} f_k^{(n)}. \end{aligned} \quad (14)$$

Hence the current decomposes naturally into its linear and higher-order parts. The n -th order contribution is

$$j_e^{s(n)} = \int [dk] (D^s)^{-1} \dot{\mathbf{r}} f_k^{(n)}. \quad (15)$$

Eq. (15) will be the basis for evaluating the linear and nonlinear transport coefficients.

A. Linear Transport

Substituting Eqs. (1) and (11) into the $n=1$ expression of Eq. (15) gives

$$\begin{aligned} \mathbf{j}_e^{s(1)} &= \frac{2\tau^*}{\tau_\nu} \int \frac{d^3k}{(2\pi)^3} [\delta\mu^s + (\epsilon^s - \mu) \frac{\delta T^s}{T}] \\ &\times \left[\frac{e}{\hbar} (\mathbf{v}^s \cdot \boldsymbol{\Omega}^s) \mathbf{B} \right] \left(-\frac{\partial f_{eq}^s}{\partial \epsilon^s} \right). \end{aligned} \quad (16)$$

For concreteness we work in the planar geometry $\mathbf{E} = E_x \hat{\mathbf{x}}$, $\nabla T = \nabla_x T \hat{\mathbf{x}}$, and a magnetic field confined to the $x-y$ plane, $\mathbf{B} = B \cos \theta \hat{\mathbf{x}} + B \sin \theta \hat{\mathbf{y}}$, with θ measured from the x -axis [Fig.(1)]. We focus on $j_y^{(1)}$ as the primary interest of this work lies in the chiral anomaly-induced planar Hall and Nernst effects, both of which manifest through the transverse current. Writing the linear response relations as $\mathbf{j}_a^{(1)} = \sum_b [\sigma_{ab} E_b - \alpha_{ab} \nabla_b T]$ and inserting Eqs. (6) and (7) into Eq. (16) yields

$$\begin{aligned} \sigma_{yx} &= -\tau^* e^2 B^2 \sin \theta \cos \theta \sum_s \left[S^{12,s} R_{12}^{01,s} C_s^0 \right. \\ &\quad \left. + S^{01,s} R_{12}^{12,s} C_s^1 \right] \end{aligned} \quad (17)$$

$$\begin{aligned} \alpha_{yx} &= -\tau^* \frac{e}{T} B^2 \sin \theta \cos \theta \sum_s \left[S^{12,s} R_{12}^{12,s} C_s^0 \right. \\ &\quad \left. + S^{01,s} R_{10}^{21,s} C_s^1 \right] \end{aligned} \quad (18)$$

where

$$R_{\gamma\delta}^{\alpha\beta,s} = \frac{C_s^\alpha}{\mathcal{D}_s^\gamma} - \frac{C_s^\beta}{\mathcal{D}_s^\delta}, \quad (19)$$

$$S^{\alpha\beta,s} = \frac{\mathcal{D}_s^\alpha \mathcal{D}_s^\beta}{\mathcal{D}_s^0 \mathcal{D}_s^2 + (\mathcal{D}_s^1)^2}, \quad (20)$$

$$C_s^\nu = \int [dk] \left(-\frac{\partial f_{eq}}{\partial \epsilon^s} \right) \frac{e}{\hbar} (\mathbf{v}^s \cdot \boldsymbol{\Omega}^s) (\epsilon^s - \mu)^\nu. \quad (21)$$

The vector relation $\Lambda_s^\nu = \mathbf{B} C_s^\nu$ connects C_s^ν to Eq. (9). The above planar coefficients scale as B^2 and have a $\sin \theta \cos \theta$ angular dependence, unlike the conventional or anomalous Hall/Nernst responses. Consequently they exhibit extrema at odd multiples of $\pi/4$ [Fig.(3)]. We now turn to the nonlinear response regime to explore higher-order contributions—in \mathbf{E} and ∇T —to the transport properties.

B. Nonlinear Transport

The second order response to external perturbations is given by

$$\mathbf{j}_e^{(2)} = -e \int [dk] (D^s)^{-1} \dot{\mathbf{r}} f_k^{(2)}, \quad (22)$$

where $f_k^{(2)}$ is the quadratic correction obtained in Eq. (12). In analogy with Eqs. (9) and (8) we introduce

$$\Sigma_s^\nu = \int [dk] \frac{\partial^2 f_{eq}}{\partial \epsilon^s \partial \epsilon^s} \frac{e}{\hbar} (\mathbf{v}^s \cdot \boldsymbol{\Omega}^s) (\epsilon^s - \mu)^\nu, \quad (23)$$

which allows Eq. (22) to be written compactly as

$$\begin{aligned} \mathbf{j}_e^{(2)} &= \frac{2eB\tau^*}{\tau_\nu} \left[(\delta\mu^s)^2 \Sigma_s^0 + 2\delta\mu^s \frac{\delta T^s}{T} (C_s^0 + \Sigma_s^1) \right. \\ &\quad \left. + \left(\frac{\delta T^s}{T} \right)^2 (2C_s^1 + \Sigma_s^2) \right] \end{aligned} \quad (24)$$

The quadratic response can be parameterized as

$$\mathbf{j}_a^{(2)} = \sum_{b,c} [\sigma_{abc} E_b E_c + \alpha_{abc} \nabla_b T \nabla_c T - \beta_{abc} E_b \nabla_c T]. \quad (25)$$

In contrast to conventional nonlinear Hall or Nernst phenomena, the chiral-anomaly mechanism generates the additional tensor β_{abc} , which encodes a mixed thermoelectric response that appears only when an electric field and a thermal gradient act simultaneously.

Combining the nonlinear current in Eq. (24) with the quadratic corrections $\delta\mu^s$ and δT^s from Eqs. (6)–(7) yields the second-order planar transport tensors

$$\begin{aligned} \sigma_{yxx} &= \frac{\tau^* \tau_\nu}{2} e^3 B^3 \cos^2 \theta \sin \theta \sum_s \left[\Sigma_s^0 (S^{12})^2 (R_{12}^{01})^2 \right. \\ &\quad \left. + (2C_s^1 + \Sigma_s^2) (S^{01})^2 (R_{10}^{10})^2 \right. \\ &\quad \left. + 2(C_s^0 + \Sigma_s^1) S^{12} S^{01} R_{12}^{01} R_{10}^{10} \right], \end{aligned} \quad (26)$$

$$\begin{aligned} \alpha_{yxx} &= \frac{\tau^* \tau_\nu}{2} \frac{e}{T^2} B^3 \cos^2 \theta \sin \theta \sum_s \left[\Sigma_s^0 (S^{12})^2 (R_{12}^{12})^2 \right. \\ &\quad \left. + (2C_s^1 + \Sigma_s^2) (S^{01})^2 (R_{10}^{21})^2 \right. \\ &\quad \left. + 2(C_s^0 + \Sigma_s^1) S^{12} S^{01} R_{12}^{12} R_{10}^{21} \right], \end{aligned} \quad (27)$$

$$\begin{aligned} \beta_{yxx} &= -\frac{\tau^* \tau_\nu}{2} \frac{e^2}{T} B^3 \cos^2 \theta \sin \theta \sum_s \left[\Sigma_s^0 (S^{12})^2 R_{12}^{01} R_{12}^{12} \right. \\ &\quad \left. + (2C_s^1 + \Sigma_s^2) (S^{01})^2 R_{10}^{10} R_{10}^{21} \right. \\ &\quad \left. + 2(C_s^0 + \Sigma_s^1) S^{12} S^{01} \right. \\ &\quad \left. \times (R_{12}^{01} R_{10}^{21} + R_{10}^{10} R_{12}^{12}) \right] \end{aligned} \quad (28)$$

The above non-linear planar transport coefficients scale as B^3 and have a $\sin \theta \cos^2 \theta$ angular dependence. Consequently they exhibit an extrema at $\theta = \arctan(1/\sqrt{2})$ [Fig.(6)]. This angle is smaller than extremum angle for the linear order case. This indicates that higher-order corrections—in \mathbf{E} and ∇T —to the transport coefficients reach their maximum at angles closer to the configuration where \mathbf{E} and ∇T are aligned with \mathbf{B} .

IV. THREE-DIMENSIONAL SPIN-ORBIT COUPLED SYSTEMS

In this section, we illustrate the general theoretical framework by applying them explicitly to a three-dimensional spin-orbit coupled metallic system. Using a model Hamiltonian, we demonstrate the emergence of chiral anomaly driven linear and nonlinear planar transport coefficients, and make several experimentally testable predictions for such systems.

A. The Hamiltonian

We model the electrons with the following effective spin-orbit-coupled Hamiltonian [105–107],

$$H = \int \frac{d^3 k}{(2\pi)^3} c_{\mathbf{k}}^\dagger \left[\frac{\hbar^2 k^2}{2m} \sigma_0 + \alpha \boldsymbol{\sigma} \cdot \mathbf{k} \right] c_{\mathbf{k}} \quad (29)$$

Here, σ_0 is the 2×2 identity matrix, the σ_i are the Pauli matrices, and $c_{\mathbf{k}}^\dagger = (c_{\mathbf{k},\uparrow}^\dagger, c_{\mathbf{k},\downarrow}^\dagger)$. Although we have adopted a simple isotropic form for the spin-orbit interaction, the chiral-anomaly and planar Hall/Nernst arguments presented above remain valid for more elaborate, anisotropic spin-orbit terms [91]. The corresponding energy eigenvalues are

$$\epsilon^s(k) = \frac{\hbar^2 k^2}{2m} + s \alpha k, \quad (30)$$

where $s = \pm 1$ labels the two bands, and $k = \|\mathbf{k}\|$. From Eq. (30), we notice that the two bands become degenerate at $\epsilon^s = 0$. This is also the minimum energy for the $s = +1$ (upper) band. The $s = -1$ (lower) band reaches its minimum energy at $-\epsilon_\alpha$, where $\epsilon_\alpha = m\alpha^2/2\hbar^2$. We focus on the regime $\mu \geq 0$, giving each band its own Fermi surface at chemical potential μ . The Chern number for each Fermi surface is

$$C_s = \iint_{\text{FS}} dS \cdot \boldsymbol{\Omega}^s = -s, \quad (31)$$

The surface integral in Eq. (31) is taken over the Fermi surface of band s . For this model the Berry curvature is

$$\boldsymbol{\Omega}_s(k) = -\frac{s}{2k^3} \mathbf{k}, \quad (32)$$

It is instructive to contrast this system with a Weyl semimetal (WSM). In a WSM, pairs of Weyl nodes with opposite chirality occur at distinct points in momentum space, directly linking nodal location to chirality. By comparison, in three-dimensional spin-orbit-coupled metals the two chiral sectors originate from the same momentum-space node yet form separate Fermi surfaces, so that chirality coincides with the band index. If instead $\mu < 0$, these Fermi pockets correspond only to the

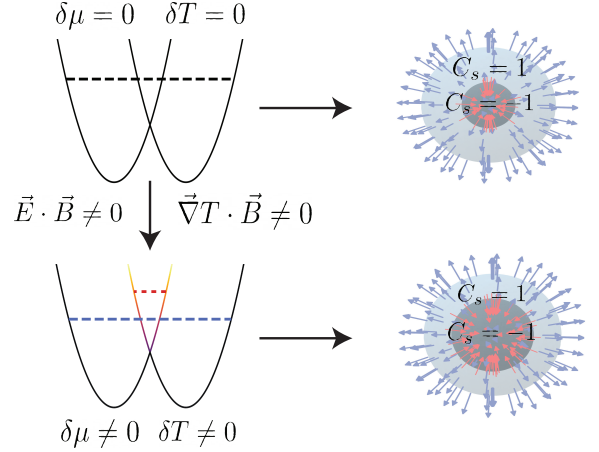


Figure 2. Band structure (left) and corresponding Fermi surfaces (right) for each chirality C_s . The arrows indicate the direction of the Berry curvature at any given point on the respective Fermi surfaces. The red ($s = 1$) band corresponds to the inner Fermi surface, while the blue ($s = -1$) band corresponds to the outer Fermi surface. With the application of a non-zero $\mathbf{E} \cdot \mathbf{B}$ or $\nabla T \cdot \mathbf{B}$ term, a chemical potential ($\delta\mu$) and temperature (δT) imbalance are created, resulting in a non-zero transverse voltage V_H (see Fig. 1).

Fermi surface for a single band, but hosting two disjoint closed surface, one with a positive band velocity, while the other has a negative band velocity; consequently $v^s \Omega^s$ changes sign between the surfaces, and the net Berry flux [Eq. (31)] vanishes. Nevertheless, one can partition the band Fermi surface into two disjoint closed regions—each carrying its own nonzero Berry flux and hence a well-defined chirality [91]—and compute the flux on each region. This procedure is identical to the separate-band calculation, except that the band index no longer serves as the chirality label. By doing so, one finds that even for $\mu < 0$ the Fermi surface contains pockets of opposite chirality, preserving the chiral anomaly. From this viewpoint, chirality can no longer be universally associated with band index. For the remainder of this paper we restrict to $\mu \geq 0$. However, for $\mu < 0$ by replacing band indices with pocket labels (corresponding to each disjoint surface), we find two chiral centers, hence the discussion made in the previous section applies to this case as well. We now proceed to compute the planar Hall and Nernst coefficients arising from the chiral anomaly.

B. Transport Properties

Below we present the analytic expressions for the fundamental moments entering the transport coefficients, as defined in Eqs. (21) and (23).

$$[C_s^0, C_s^1, C_s^2] = -\frac{se}{4\pi^2 \hbar^2} [F_0, \frac{1}{\beta} F_1, \frac{1}{\beta^2} F_2] \quad (33)$$

$$[\Sigma_s^0, \Sigma_s^1, \Sigma_s^2] = -\frac{se}{4\pi^2\hbar^2} [G_0, \frac{1}{\beta}G_1, \frac{1}{\beta^2}G_2] \quad (34)$$

where,

$$F^0(x_s) = \frac{1}{1 + e^{-x_s}} \quad (35)$$

$$F^1(x_s) = \frac{x_s}{1 + e^{x_s}} + \ln(1 + e^{-x_s}) \quad (36)$$

$$\begin{aligned} F^2(x_s) = & \frac{\pi^2}{3} - x \left(\frac{x_s}{1 + e^{x_s}} + 2 \ln(1 + e^{-x_s}) \right) \\ & + 2 \text{Li}_2(-e^{-x_s}) \end{aligned} \quad (37)$$

$$G^0(x_s) = \frac{\beta e^{-x_s}}{(1 + e^{-x_s})^2} \quad (38)$$

$$G^1(x_s) = -\frac{\beta x_s e^{-x_s}}{(1 + e^{-x_s})^2} + \frac{\beta}{1 + e^{-x_s}} \quad (39)$$

$$\begin{aligned} G^2(x_s) = & \frac{\beta x_s^2 e^{-x_s}}{(1 + e^{-x_s})^2} + \frac{2\beta x_s}{1 + e^{-x_s}} \\ & + 2\beta \ln(1 + e^{-x_s}) \end{aligned} \quad (40)$$

Here, $x_{-1} = \beta\mu$ and $x_1 = \beta(\mu + \epsilon_\alpha)$, and $\text{Li}_2(x)$ denotes the dilogarithm function. In the low temperature limit $\beta\mu \gg 1$ (i.e. $x_s \gg 1$), one finds $F^0 \rightarrow 1$, $F^2 \rightarrow \pi^2/3$, and $G^1 \rightarrow \beta$, while all other functions decay exponentially. Accordingly, in the low-temperature regime $\beta\mu \gg 1$, keeping only the leading terms in T , the moments D_s^ν reduce to:

$$\begin{bmatrix} D_s^0 \\ D_s^1 \\ D_s^2 \end{bmatrix} = -\frac{m^{\frac{3}{2}}\sqrt{\epsilon_\alpha}}{\sqrt{2}\pi^2\hbar^3} \begin{bmatrix} \left(\frac{(1-s\sqrt{1+\tilde{\mu}})^2}{\sqrt{1+\tilde{\mu}}} \right) F_0 \\ \left(\frac{\tilde{\mu}}{2\beta^2\epsilon_\alpha(1+\tilde{\mu})^{\frac{3}{2}}} \right) F_2 \\ \frac{1}{\beta^2} \left(\frac{(1-s\sqrt{1+\tilde{\mu}})^2}{\sqrt{1+\tilde{\mu}}} \right) F_2 \end{bmatrix} \quad (41)$$

Retaining only the leading temperature-dependent terms, the linear planar transport coefficients are given by:

$$\begin{aligned} \sigma_{yx}^{LT} = & \left(\frac{\tau^* e^4}{4\sqrt{2}\pi^2\hbar m^{\frac{3}{2}}\sqrt{\epsilon_\alpha}} \right) B^2 \cos(\theta) \sin(\theta) \\ & \times \left[\frac{(2 + \tilde{\mu})\sqrt{1 + \tilde{\mu}}}{\tilde{\mu}^2} \right] \end{aligned} \quad (42)$$

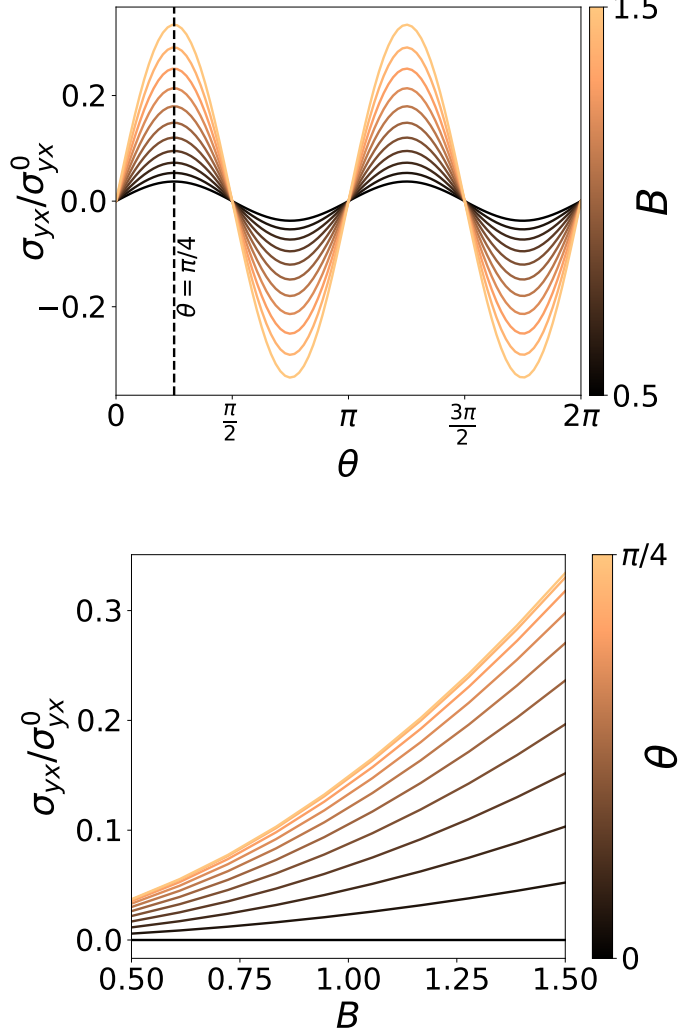


Figure 3. Normalized planar Hall conductivity $\sigma_{yx}/\sigma_{yx}^0$ (with $\sigma_{yx}^0 = \frac{\tau^* e^4}{8\sqrt{2}\pi^2\hbar m^{\frac{3}{2}}\epsilon_\alpha^{\frac{1}{2}}}$) as a function of (top) the angle θ between the magnetic field and current for field strengths $0.5 \leq B \leq 1.5$ (color scale), and (bottom) the field magnitude B for angles $0 \leq \theta \leq \pi/4$ (color scale). We can notice that the maximum value for the field strength occurs when $\theta = \pi/4$.

$$\begin{aligned} \alpha_{yx}^{LT} = & \left(\frac{\tau^* e^3 k_B}{24\sqrt{2}\beta\hbar m^{\frac{3}{2}}\epsilon_\alpha^{\frac{3}{2}}} \right) B^2 \cos(\theta) \sin(\theta) \\ & \times \left[\frac{\tilde{\mu}^2 + 8\tilde{\mu} + 8}{\tilde{\mu}^3\sqrt{1 + \tilde{\mu}}} \right] \end{aligned} \quad (43)$$

We begin by highlighting key features of the anomaly-induced planar transport coefficients. Fig. 3 (top) shows the planar Hall coefficient σ_{yx} (from Eq. (17)) versus the angle θ between the magnetic and electric fields, for several magnetic-field strengths. The $\sin \theta \cos \theta$ dependence produces extrema at odd multiples of $\pi/4$, and σ_{yx} van-

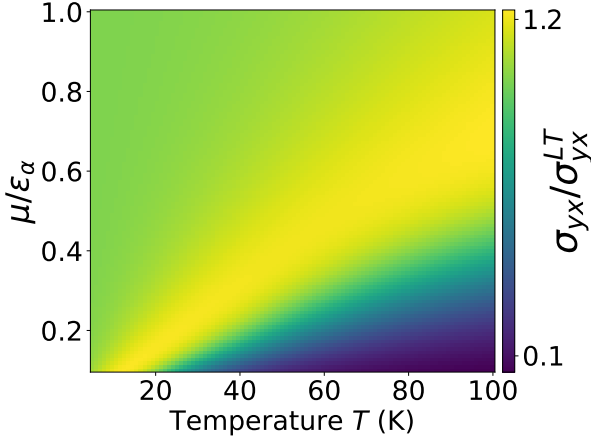


Figure 4. Heatmap of the validity of the low-temperature expansion for the linear transverse conductivity. The color scale shows the ratio $\sigma_{yx}/\sigma_{yx}^{LT}$ as a function of temperature T and rescaled chemical potential μ/ϵ_α . Unity (green) denotes exact agreement with the analytic result, while deviations (yellow to purple) indicate breakdown of the expansion. The low-temperature approximation fails most strongly at low μ/ϵ_α and high T .

ishes when $\mathbf{B} \perp \mathbf{E}$. The planar transverse response also vanishes when $\mathbf{B} \parallel \mathbf{E}$. Fig. 3 (bottom) demonstrates the quadratic scaling $\sigma_{yx} \propto B^2$, a signature of anomaly-driven planar transport. Although only the planar Hall response is plotted here, the planar Nernst coefficient exhibits the same angular and B -field dependence.

Although the low-temperature forms given in Eqs. (42) and (43) satisfy the Mott relation [99] ($\alpha \propto T \partial_\mu \sigma$), a closer look at certain fundamental moments—e.g. Eq. (36)—reveals leading-order terms that decay exponentially in T , thereby violating the Mott relation even at relatively low temperatures. Fig. 4 shows the validity of low-temperature expansion for the linear transverse conductivity (Eq.(42)) for varying normalized chemical potential μ/ϵ_α and temperature T . The ratio $\sigma_{yx}/\sigma_{yx}^{LT}$ remains unity (green shading) in the low-temperature, large- μ/ϵ_α regime, indicating agreement with the low temperature expansion. The onset of departure appears as a yellow-to-blue gradient, marking where the full calculation deviates from its low- T approximation. At small μ/ϵ_α , even modest temperatures T suffice to drive the system into the deviation region, whereas at higher μ/ϵ_α the low-temperature form holds up to larger T . To further understand the validity of the low temperature expansion, Fig. 5 shows a plot comparing the Mott number ($\mathcal{M} = \frac{\alpha}{T \partial_\mu \sigma}$) rescaled to unity in the low temperature limit, computed numerically (purple line) with its expected value (green line). A Mott number value close to unity indicates agreement with the Mott relation, while a deviation signals a breakdown of this approximation. We can see that the Mott relation is not valid for higher temperatures and the deviation is apparent at fairly low

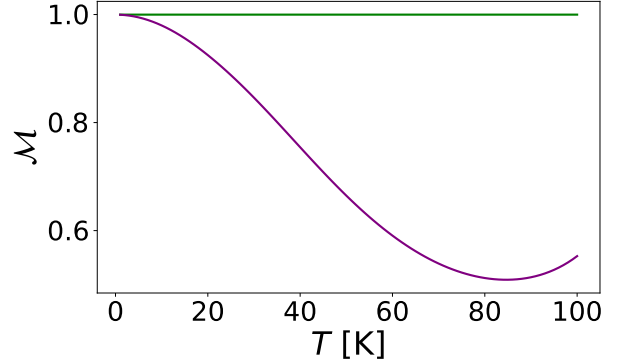


Figure 5. Variation of the Mott number as a function of temperature. *Solid purple line:* Numerical result for the Mott number $\mathcal{M} = \alpha_{yx}/(T \partial_\mu \sigma_{yx})$. *Solid green line:* Expected value of the Mott number scaled to unity. The departure of \mathcal{M} from unity at higher temperatures highlights the violation of the Mott relation.

temperatures (approximately 10% deviation at 20K from the ideal value). This violation at relatively low temperatures arises from the exponential behavior of the fundamental moments with respect to temperature (Eqs.(35)-(37)), in contrast to the polynomial dependence assumed in the conventional Mott relation derived via the Sommerfeld expansion [99].

We now turn to the second-order transport coefficients. By substituting Eqs. (26)–(28) into our Hamiltonian's expressions and retaining only the leading terms as $T \rightarrow 0$, we find:

$$\begin{aligned} \sigma_{yxx}^{LT} = & (\tau^* \tau_\nu) \left(\frac{e^6}{32\pi^2 m^3 \epsilon_\alpha} \right) B^3 \cos^2(\theta) \sin(\theta) \\ & \times \left[\frac{12(1+\tilde{\mu})^{\frac{1}{2}} + 40(1+\tilde{\mu})^{\frac{3}{2}} + 12(1+\tilde{\mu})^{\frac{5}{2}}}{\tilde{\mu}^5} \right] \end{aligned} \quad (44)$$

$$\begin{aligned} \alpha_{yxx}^{LT} = & (\tau^* \tau_\nu) \left(\frac{e^4 k_B}{96m^3 \epsilon_\alpha} \right) B^3 \cos^2(\theta) \sin(\theta) \\ & \times \left[\frac{12(1+\tilde{\mu})^{\frac{1}{2}} + 40(1+\tilde{\mu})^{\frac{3}{2}} + 12(1+\tilde{\mu})^{\frac{5}{2}}}{\tilde{\mu}^5} \right] \end{aligned} \quad (45)$$

$$\begin{aligned} \beta_{yxx}^{LT} = & (\tau^* \tau_\nu) \left(\frac{e^5}{2\pi^2 m^3 T} \right) B^3 \cos^2(\theta) \sin(\theta) \\ & \times \left[\frac{(1+\tilde{\mu})^{\frac{1}{2}} + (1+\tilde{\mu})^{\frac{3}{2}}}{\tilde{\mu}^4} \right] \end{aligned} \quad (46)$$

In the second-order regime, we observe several new features that distinguish nonlinear planar transport from its linear counterpart. Fig. 6 (top) displays the second-order planar Hall coefficient σ_{yxx} versus the angle θ between \mathbf{B}

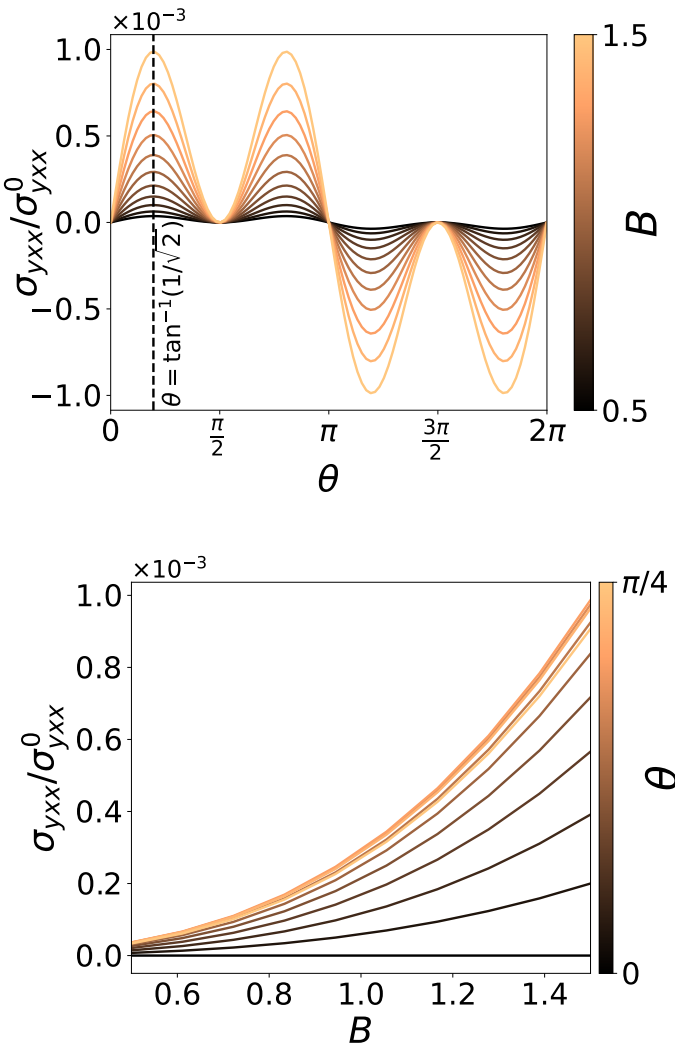


Figure 6. Non-linear normalized planar Hall conductivity $\sigma_{yxx}/\sigma_{yxx}^0$ (with $\sigma_{yxx}^0 = \frac{\tau_0 \pi^2 e^6}{32\pi^2 m^3 \epsilon_\alpha^2}$) as a function of (top) the in-plane field angle θ for $0.5 \leq B \leq 1.5$ (color bar), with the linear-response peak at $\theta = \pi/4$ indicated by a dashed line; and (bottom) the field magnitude B for $0 \leq \theta \leq \pi/4$ (color bar). Unlike the linear response (Fig. 3), the non-linear conductivity reaches its maximum at $\theta = \tan^{-1}(1/\sqrt{2}) < \pi/4$

and \mathbf{E} for several magnetic-field strengths. As expected, σ_{yxx} vanishes at $\theta = \pi/2$ when $\mathbf{B} \perp \mathbf{E}$. Remarkably, it remains positive up to $\theta = \pi$ and then switches sign, remaining negative until 2π , thus exhibiting a 2π periodicity rather than the π period seen in the linear response. Although not shown, all higher-order planar coefficients share this 2π periodicity. The peak shifts from $\theta = \pi/4$ to $\theta = \arctan(1/\sqrt{2})$, consistent with the $\cos^2 \theta \sin \theta$ angular form of the second-order response. More generally, an n th-order coefficient varies as $\cos^n \theta \sin \theta$, placing its extremum at $\theta = \arctan(1/\sqrt{n})$ and rapidly suppressing the amplitude once \mathbf{B} and \mathbf{E} deviate from parallel. Fig.

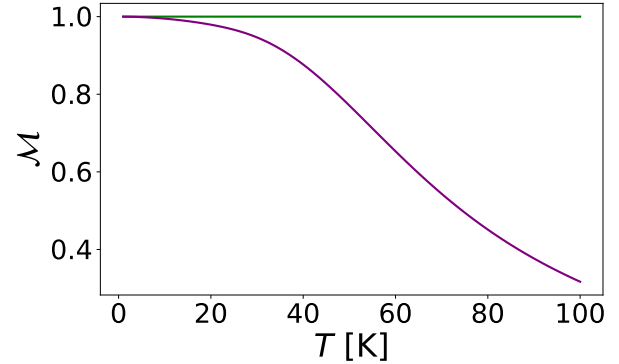


Figure 7. Variation of the non-linear Mott number as a function of temperature. *Solid purple line:* Numerical result for the non-linear Mott number $\mathcal{M} = \alpha_{yxx}/\sigma_{yxx}$. *Solid green line:* Expected value of the non-linear Mott number scaled to unity. The departure of \mathcal{M} from unity at higher temperatures highlights the violation of the non-linear Mott relation.

6 (bottom) shows $\sigma_{yxx} \propto B^3$, in contrast to the quadratic B^2 scaling of the linear effect; indeed, the n th-order term scales as B^{n+1} . The plot also shows the magnetic field variation for θ values ranging from $\theta = 0$ to $\theta = \pi/4$ with a color gradient. The peaking of the transport coefficient at an angle smaller than $\pi/4$ is evident from this plot. A new feature of our calculations in the nonlinear order is the emergence of a mixed transport coefficient β which gives rise to a transverse current proportional to both \mathbf{E} and ∇T (see Eq.(25)). This quantity can be experimentally demonstrated in the spin-orbit coupled metallic system in the presence of chiral anomaly by having a coplanar temperature gradient, electric field, and magnetic field simultaneously non-zero in the 3D system and measuring the current transverse to the electric field proportional to both \mathbf{E} and ∇T . The nonlinear Nernst and the mixed thermoelectric coefficients obey the same angular and field-strength dependence.

Substituting the exact low- T expressions from Eqs.(44) and (45) shows

$$\alpha_{yxx}^{LT} = \left(\frac{\pi^2 k_B^2}{3e^2} \right) \sigma_{yxx}^{LT}, \quad (47)$$

confirming the validity of the non-linear analog of the Mott relation [100, 101]. The same conclusion is revealed from Fig. 7, which shows the normalized Mott number $\mathcal{L} = \alpha_{yxx}/\sigma_{yxx}$ as a function of temperature. As predicted, \mathcal{M} remains constant at low T and then deviates at higher T . In the non-linear case however, the non-linear Mott relation is valid for temperatures higher than its linear counterpart (approximately 10% deviation at 40K from the ideal value). We also stress that no simple Wiedemann–Franz or Mott-type proportionality can link the mixed thermoelectric coefficient β to the other non-linear planar transport coefficients. Now turning to the mixed thermoelectric transport coefficient, Fig. 8

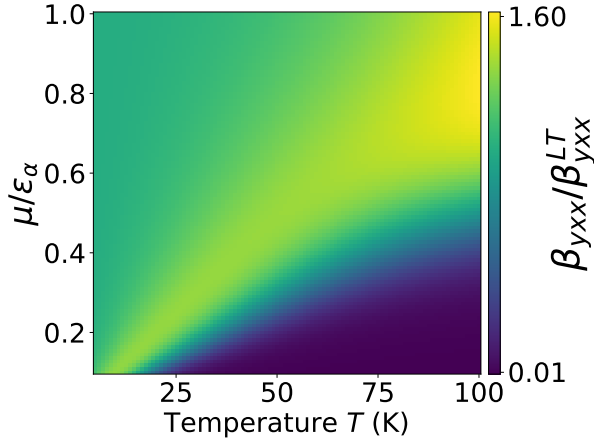


Figure 8. Heatmap of the low-temperature expansion validity for the non-linear electrothermal coefficient. The color scale shows the ratio $\beta_{yxx}/\beta_{yxx}^{LT}$ plotted against temperature T and rescaled chemical potential μ/ϵ_α . Unity (green) indicates exact agreement with the analytic low- T form, while deviations (yellow to purple) mark the breakdown of the expansion at low μ/ϵ_α and elevated T .

shows a heatmap of the ratio $\beta_{yxx}/\beta_{yxx}^{LT}$ as a function of the temperature T and the scaled chemical potential μ/ϵ_α . Similar to the linear case, we note that at small μ/ϵ_α , even a small temperature is sufficient to result in a violation of the low temperature expansion, whereas at larger μ/ϵ_α , a sufficiently larger temperature is necessary to result in a violation.

V. CONCLUSION

In this paper, we have investigated linear and nonlinear planar transport phenomena driven by the chiral anomaly in three-dimensional spin-orbit coupled metallic systems, employing a semiclassical Boltzmann transport formalism up to second order in the applied fields. Unlike conventional Weyl semimetals, these systems host distinct Fermi surfaces characterized by opposite Berry curvature fluxes without explicit band degeneracies at the Fermi energy. Our theoretical framework highlights novel anomaly-driven transport responses, which can be experimentally accessed through planar Hall, planar Nernst, and mixed nonlinear electrothermal effects.

In the linear regime, we have shown that the anomaly-induced planar transport coefficients $(\sigma_{yx}, \alpha_{yx})$ exhibit a $\sin \theta \cos \theta$ angular dependence and scale quadratically with the applied magnetic field. Notably, our detailed numerical analysis reveals a clear breakdown of the Mott relation at relatively low temperatures. This violation arises from the exponential dependence of the fundamental moments contributing to the transport coefficients, rather than the polynomial temperature dependence assumed in conventional derivations.

Extending our analysis to the nonlinear regime, A new

feature of our calculations in the nonlinear order is the emergence of a mixed transport coefficient β (see Eq.(46)) which gives rise to a transverse current proportional to both \mathbf{E} and ∇T (see Eq.(25)). This quantity can be experimentally demonstrated in the spin-orbit coupled metallic system in the presence of chiral anomaly by having a coplanar temperature gradient, electric field, and magnetic field simultaneously non-zero in the 3D system and measuring the current transverse to the electric field proportional to both \mathbf{E} and ∇T . These nonlinear planar responses exhibit a distinct angular dependence—with peaks shifted from $\pi/4$ to smaller angles—and display a stronger cubic scaling with magnetic field strength. Furthermore, due to the exponential temperature dependence of the transport coefficients, we observe significant deviations from the nonlinear Mott relation at temperatures well below the regime where the polynomial expansion remains valid.

These theoretical predictions can be directly tested through planar transport measurements under the simultaneous application of electric fields and thermal gradients. Such experiments would not only validate our theoretical results but also establish clear signatures of chiral anomaly-driven transport in spin-orbit coupled metallic systems.

VI. ACKNOWLEDGMENT

S.T., R.G.G and B.B.R. acknowledge support from SC Quantum, ARO W911NF2210247 and ONR-N000142312061. G.S. was supported by ANRF-SERB Core Research Grant CRG/2023/005628. G.S. thanks Azaz Ahmad and Gautham Varma K. for useful discussions.

Appendix A: CALCULATION OF THE FIRST AND SECOND ORDER PERTURBATION TERMS

To calculate the correction terms, let's start with the collision term in the transport equation,

$$I_{coll} = - \left(\frac{\delta f_k^s}{\tau^*} \right) - \left(\frac{f_{eq}(\epsilon^s, \mu^s, T^s) - f_{eq}(\epsilon^s, \mu^{\bar{s}}, T^{\bar{s}})}{\tau_\nu} \right) \quad (A1)$$

Using the definition of δT^s and $\delta\mu^s$ on the second term in the collision equation we obtain,

$$\begin{aligned} f_{eq}(\epsilon^s, \mu^{\bar{s}}, T^{\bar{s}}) &= f_{eq}(\epsilon^s, \mu^s - 2\delta\mu^s, T^s - 2\delta T^s) \\ \implies f_{eq}(\epsilon^s, \mu^{\bar{s}}, T^{\bar{s}}) &= f_{eq}(\epsilon^s, \mu^s, T^s) - 2 \left(\frac{\partial f_{eq}}{\partial \mu} \right) \delta\mu^s \\ &\quad - 2 \left(\frac{\partial f_{eq}}{\partial T} \right) \delta T^s + [\delta\mu^s \ \delta T^s] \begin{bmatrix} \frac{\partial^2 f_{eq}}{\partial \mu^2} & \frac{\partial^2 f_{eq}}{\partial \mu \partial T} \\ \frac{\partial^2 f_{eq}}{\partial \mu \partial T} & \frac{\partial^2 f_{eq}}{\partial T^2} \end{bmatrix} \begin{bmatrix} \delta\mu^s \\ \delta T^s \end{bmatrix} \end{aligned} \quad (\text{A2})$$

The second and third terms on the right-hand side correspond to the first-order deviation ($f_D^{(1)}$) of $f_{eq}(\epsilon^s, \mu^{\bar{s}}, T^{\bar{s}})$ from $f_{eq}(\epsilon^s, \mu^s, T^s)$, and the third term, also called the Hessian, corresponds to the second-order deviation ($f_D^{(2)}$). Now, using the fact that $\frac{\partial f_{eq}}{\partial \mu} = -\frac{\partial f_{eq}}{\partial \epsilon^s}$ and $\frac{\partial f_{eq}}{\partial T} = -\frac{\partial f_{eq}}{\partial \epsilon^s} \left(\frac{\epsilon^s - \mu}{T} \right)$, we obtain,

$$f_D^{(1)} = 2 \left(\frac{\partial f_{eq}}{\partial \epsilon^s} \right) \delta\mu^s + 2 \left(\frac{\partial f_{eq}}{\partial \epsilon^s} \right) \left(\frac{\epsilon^s - \mu}{T} \right) \delta T^s \quad (\text{A3})$$

$$\begin{aligned} f_D^{(2)} &= 2 \left(\frac{\partial^2 f_{eq}}{\partial \epsilon^s \partial \epsilon^s} \right) (\delta\mu^s)^2 + 4 \left[\frac{1}{T} \left(\frac{\partial f_{eq}}{\partial \epsilon^s} \right) \right. \\ &\quad \left. + \left(\frac{\epsilon^s - \mu}{T} \right) \left(\frac{\partial^2 f_{eq}}{\partial \epsilon^s \partial \epsilon^s} \right) \right] (\delta\mu^s)(\delta T^s) \\ &\quad + 2 \left[2 \left(\frac{\epsilon^s - \mu}{T^2} \right) \left(\frac{\partial f_{eq}}{\partial \epsilon^s} \right) \right. \\ &\quad \left. + \left(\frac{\epsilon^s - \mu}{T} \right)^2 \left(\frac{\partial^2 f_{eq}}{\partial \epsilon^s \partial \epsilon^s} \right) \right] (\delta T^s)^2 \end{aligned} \quad (\text{A4})$$

Thus, the correction equations can be collectively written as,

$$\begin{aligned} D \left(\mathbf{v}^s + \frac{e}{\hbar} (\mathbf{v}^s \cdot \boldsymbol{\Omega}^s) \mathbf{B} \right) \cdot \left(e \mathbf{E} + \left(\frac{\epsilon^s - \mu}{T} \right) \boldsymbol{\nabla} T \right) \\ \times \left(- \frac{\partial(f_{eq}^s + f_k^{(1)} + f_k^{(2)} + \dots)}{\partial \epsilon^s} \right) = - \left(\frac{\delta(f_k^{(1)} + f_k^{(2)} + \dots)}{\tau^*} \right) f_k^{(1)} = - \tau^* D \left[\mathbf{v}^s + \frac{e}{\hbar} (\mathbf{v}^s \cdot \boldsymbol{\Omega}^s) \mathbf{B} \right] \cdot \left[e \mathbf{E} + \left(\frac{\epsilon^s - \mu}{T} \right) \boldsymbol{\nabla} T \right] \\ - \left(\frac{f_{eq}(\epsilon^s, \mu^s, T^s) - f_{eq}(\epsilon^s, \mu^{\bar{s}}, T^{\bar{s}})}{\tau_\nu} \right) \end{aligned} \quad (\text{A5})$$

We obtain the correction terms by comparing terms of even order on both sides of the above equation. Now, to obtain the values of $\delta\mu^s$ and δT^s , we only consider the

first-order contribution in equation (A5).

$$\begin{aligned} D \left(\mathbf{v}^s + \frac{e}{\hbar} (\mathbf{v}^s \cdot \boldsymbol{\Omega}^s) \mathbf{B} \right) \cdot \left(e \mathbf{E} + \left(\frac{\epsilon^s - \mu}{T} \right) \boldsymbol{\nabla} T \right) \left(- \frac{\partial f_{eq}^s}{\partial \epsilon^s} \right) \\ = - \left(\frac{\delta f_k^{(1)}}{\tau^*} \right) - \frac{2}{\tau_\nu} \left(\frac{\partial f_{eq}}{\partial \epsilon^s} \right) \left[\delta\mu^s + \left(\frac{\epsilon^s - \mu}{T} \right) \right] \end{aligned} \quad (\text{A6})$$

Integrating this equation over the Brillouin zone and using the definitions (9) and (8), we have,

$$-\frac{\tau_\nu}{2} \left(e \mathbf{E} \cdot \mathbf{\Lambda}_s^0 + \frac{\boldsymbol{\nabla} T}{T} \cdot \mathbf{\Lambda}_s^1 \right) = (\delta\mu^s) D_s^0 + \left(\frac{\delta T^s}{T} \right) D_s^1 \quad (\text{A7})$$

The integral of the first term on the right-hand side of equation (A6) vanishes since it is the integration over all the perturbations in the Brillouin zone. We can obtain an equation similar to (A7) by multiplying equation (A6) by $(\epsilon^s - \mu)$.

$$-\frac{\tau_\nu}{2} \left(e \mathbf{E} \cdot \mathbf{\Lambda}_s^1 + \frac{\boldsymbol{\nabla} T}{T} \cdot \mathbf{\Lambda}_s^2 \right) = (\delta\mu^s) D_s^1 + \left(\frac{\delta T^s}{T} \right) D_s^2 \quad (\text{A8})$$

Solving for $\delta\mu^s$ and δT^s , we finally obtain,

$$\begin{aligned} \delta\mu^s &= - \frac{\tau_\nu}{2} \left(\frac{D_s^1 D_s^2}{D_s^0 D_s^2 - (D_s^1)^2} \right) \left[\left(\frac{\mathbf{\Lambda}_s^0}{D_s^1} - \frac{\mathbf{\Lambda}_s^1}{D_s^2} \right) \cdot e \mathbf{E} \right. \\ &\quad \left. + \left(\frac{\mathbf{\Lambda}_s^1}{D_s^1} - \frac{\mathbf{\Lambda}_s^2}{D_s^2} \right) \cdot \frac{\boldsymbol{\nabla} T}{T} \right] \end{aligned} \quad (\text{A9})$$

$$\begin{aligned} \frac{\delta T^s}{T} &= - \frac{\tau_\nu}{2} \left(\frac{D_s^0 D_s^1}{D_s^0 D_s^2 - (D_s^1)^2} \right) \left[\left(\frac{\mathbf{\Lambda}_s^1}{D_s^1} - \frac{\mathbf{\Lambda}_s^2}{D_s^2} \right) \cdot e \mathbf{E} \right. \\ &\quad \left. + \left(\frac{\mathbf{\Lambda}_s^2}{D_s^1} - \frac{\mathbf{\Lambda}_s^1}{D_s^0} \right) \cdot \frac{\boldsymbol{\nabla} T}{T} \right] \end{aligned} \quad (\text{A10})$$

Finally, from equation A6, we obtain the first-order correction term as follows:

$$\begin{aligned} \delta(f_k^{(1)} + f_k^{(2)} + \dots) &= - \tau^* D \left[\mathbf{v}^s + \frac{e}{\hbar} (\mathbf{v}^s \cdot \boldsymbol{\Omega}^s) \mathbf{B} \right] \cdot \left[e \mathbf{E} + \left(\frac{\epsilon^s - \mu}{T} \right) \boldsymbol{\nabla} T \right] \\ &\quad \times \left(\frac{\partial f_{eq}}{\partial \epsilon^s} \right) - 2 \left(\frac{\tau^*}{\tau_\nu} \right) \left(\frac{\partial f_{eq}}{\partial \epsilon^s} \right) \\ &\quad \times \left[\delta\mu^s + \left(\frac{\epsilon^s - \mu}{T} \right) \delta T^s \right] \end{aligned} \quad (\text{A11})$$

Now, to obtain the second order correction, the correction equation is simply modified into,

$$\begin{aligned}
& D \left(\mathbf{v}^s + \frac{e}{\hbar} (\mathbf{v}^s \cdot \boldsymbol{\Omega}^s) \mathbf{B} \right) \cdot \left(e \mathbf{E} + \left(\frac{\epsilon^s - \mu}{T} \right) \boldsymbol{\nabla} T \right) \\
& \times \left(-\frac{\partial f_k^{(1)}}{\partial \epsilon^s} \right) = - \left(\frac{\delta f_k^{(2)}}{\tau^*} \right) - \frac{2}{\tau_\nu} \left[\left(\frac{\partial^2 f_{eq}}{\partial \epsilon^{s2}} \right) (\delta \mu^s)^2 \right. \\
& \left. + 2 \left(\frac{1}{T} \left(\frac{\partial f_{eq}}{\partial \epsilon^s} \right) + \left(\frac{\epsilon^s - \mu}{T} \right) \left(\frac{\partial^2 f_{eq}}{\partial \epsilon^{s2}} \right) \right) (\delta \mu^s) (\delta T^s) \right] \\
& + \frac{2}{\tau_\nu} \left[2 \left(\frac{\epsilon^s - \mu}{T^2} \right) \left(\frac{\partial f_{eq}}{\partial \epsilon^s} \right) \right. \\
& \left. + \left(\frac{\epsilon^s - \mu}{T} \right)^2 \left(\frac{\partial^2 f_{eq}}{\partial \epsilon^{s2}} \right) \right] (\delta T^s)^2
\end{aligned} \tag{A12}$$

Using equations (A11) and (A12), we obtain the second-order correctionas,

$$\begin{aligned}
f_k^{(2)} = & + (\tau^*)^2 D^2 \left[\mathbf{v}^s \cdot \left(e \mathbf{E} + \left(\frac{\epsilon^s - \mu}{T} \right) \boldsymbol{\nabla} T \right) \right] \times \left(\mathbf{v}^s \cdot \left(\frac{\boldsymbol{\nabla} T}{T} \right) \right) \left(\frac{\partial f_{eq}}{\partial \epsilon^s} \right) \\
& + (\tau^*)^2 D^2 \left[\mathbf{v}^s \cdot \left(e \mathbf{E} + \left(\frac{\epsilon^s - \mu}{T} \right) \boldsymbol{\nabla} T \right) \right]^2 \left(\frac{\partial^2 f_{eq}}{\partial \epsilon^{s2}} \right) \\
& + 2 \left(\frac{(\tau^*)^2}{\tau_\nu} \right) D \left[\left(\frac{\delta T^s}{T} \right) \left(\frac{\partial f_{eq}}{\partial \epsilon^s} \right) + \left(\delta \mu^s + \left(\frac{\epsilon^s - \mu}{T} \right) \delta T^s \right) \left(\frac{\partial^2 f_{eq}}{\partial \epsilon^{s2}} \right) \right] \\
& - 2 \left(\frac{\tau^*}{\tau_\nu} \right) \left[\left(\frac{\partial^2 f_{eq}}{\partial \epsilon^{s2}} \right) (\delta \mu^s)^2 + \frac{2}{T} \left(\left(\frac{\partial f_{eq}}{\partial \epsilon^s} \right) + (\epsilon^s - \mu) \left(\frac{\partial^2 f_{eq}}{\partial \epsilon^{s2}} \right) \right) (\delta \mu^s) (\delta T^s) \right] \\
& - 2 \left(\frac{\tau^*}{\tau_\nu} \right) \left[\frac{2}{T^2} (\epsilon^s - \mu) \left(\frac{\partial f_{eq}}{\partial \epsilon^s} \right) + \frac{1}{T^2} (\epsilon^s - \mu)^2 \left(\frac{\partial^2 f_{eq}}{\partial \epsilon^{s2}} \right) \right] (\delta T^s)^2
\end{aligned} \tag{A13}$$

In the chiral limit, where $\tau_\nu \gg \tau^*$, we have,

$$\begin{aligned}
f_k^{(2)} = & - 2 \left(\frac{\tau^*}{\tau_\nu} \right) \left[\left(\frac{\partial^2 f_{eq}}{\partial \epsilon^{s2}} \right) (\delta \mu^s)^2 + \frac{2}{T} \left(\left(\frac{\partial f_{eq}}{\partial \epsilon^s} \right) + (\epsilon^s - \mu) \left(\frac{\partial^2 f_{eq}}{\partial \epsilon^{s2}} \right) \right) (\delta \mu^s) (\delta T^s) \right] \\
& - 2 \left(\frac{\tau^*}{\tau_\nu} \right) \left[\frac{2}{T^2} (\epsilon^s - \mu) \left(\frac{\partial f_{eq}}{\partial \epsilon^s} \right) + \frac{1}{T^2} (\epsilon^s - \mu)^2 \left(\frac{\partial^2 f_{eq}}{\partial \epsilon^{s2}} \right) \right] (\delta T^s)^2
\end{aligned} \tag{A14}$$

This equation will be used to derive the current and the various transport coefficients associated with it.

[1] M. Z. Hasan and C. L. Kane, *Rev. Mod. Phys.* **82**, 3045 (2010).

[2] X.-L. Qi and S.-C. Zhang, *Rev. Mod. Phys.* **83**, 1057

- (2011).
- [3] N. P. Armitage, E. J. Mele, and A. Vishwanath, *Rev. Mod. Phys.* **90**, 015001 (2018).
 - [4] S. Jia, S.-Y. Xu, and M. Z. Hasan, *Nat. Mater.* **15**, 1140 (2016).
 - [5] X. Wan, A. M. Turner, A. Vishwanath, and S. Y. Savrasov, *Phys. Rev. B* **83**, 205101 (2011).
 - [6] A. A. Burkov, *Phys. Rev. Lett.* **113**, 247203 (2014).
 - [7] T. Bauer, F. Buccheri, A. De Martino, and R. Egger, *Phys. Rev. Research* **6**, 10.1103/physrevresearch.6.043201 (2024).
 - [8] M. E. Peskin and D. V. Schroeder, *An Introduction to quantum field theory* (Addison-Wesley, Reading, USA, 1995).
 - [9] G. Xu, H. Weng, Z. Wang, X. Dai, and Z. Fang, *Phys. Rev. Lett.* **107**, 186806 (2011).
 - [10] A. A. Burkov, M. D. Hook, and L. Balents, *Phys. Rev. B* **84**, 235126 (2011).
 - [11] A. A. Burkov and L. Balents, *Phys. Rev. Lett.* **107**, 127205 (2011).
 - [12] C. Fang, M. J. Gilbert, X. Dai, and B. A. Bernevig, *Phys. Rev. Lett.* **108**, 266802 (2012).
 - [13] P. Hosur, S. A. Parameswaran, and A. Vishwanath, *Phys. Rev. Lett.* **108**, 046602 (2012).
 - [14] S. Saha and S. Tewari, *The Eur. Phys. J. B* **91**, 4 (2018).
 - [15] S. M. Young, S. Zaheer, J. C. Y. Teo, C. L. Kane, E. J. Mele, and A. M. Rappe, *Phys. Rev. Lett.* **108**, 140405 (2012).
 - [16] Z. Wang, Y. Sun, X.-Q. Chen, C. Franchini, G. Xu, H. Weng, X. Dai, and Z. Fang, *Phys. Rev. B* **85**, 195320 (2012).
 - [17] B. Yang and N. Nagaosa, *Nat. Commun.* **5**, <https://doi.org/10.1038/ncomms5898> (2014).
 - [18] F. Le Mardelé, J. Wyzula, I. Mohelsky, S. Nasrallah, M. Loh, S. Ben David, O. Toledano, D. Tolj, M. Novak, G. Eguchi, S. Paschen, N. Barisić, J. Chen, A. Kimura, M. Orlita, Z. Rukelj, A. Akrap, and D. Santos-Cottin, *Phys. Rev. B* **107**, L241101 (2023).
 - [19] B. J. Wieder, Z. Wang, J. Cano, X. Dai, L. M. Schoop, B. Bradlyn, and B. A. Bernevig, *Nat. Commun.* **11**, 627 (2020).
 - [20] A. H. Castro Neto, F. Guinea, N. M. R. Peres, K. S. Novoselov, and A. K. Geim, *Rev. Mod. Phys.* **81**, 109 (2009).
 - [21] T. Sato, K. Segawa, K. Kosaka, S. Souma, K. Nakayama, K. Eto, T. Minami, Y. Ando, and T. Takahashi, *Nat. Phys.* **7**, 840 (2011).
 - [22] Z. K. Liu, B. Zhou, Y. Zhang, Z. J. Wang, H. M. Weng, D. Prabhakaran, S.-K. Mo, Z. X. Shen, Z. Fang, X. Dai, Z. Hussain, and Y. L. Chen, *Science* **343**, 864–867 (2014).
 - [23] S. Jeon, B. B. Zhou, A. Gynis, B. E. Feldman, I. Kimchi, A. C. Potter, Q. D. Gibson, R. J. Cava, A. Vishwanath, and A. Yazdani, *Nature Materials* **13**, 851–856 (2014).
 - [24] T. Morimoto and A. Furusaki, *Phys. Rev. B* **89**, 235127 (2014).
 - [25] G. Sharma, C. Moore, S. Saha, and S. Tewari, *Phys. Rev. B* **96**, 195119 (2017).
 - [26] L. Fu and C. L. Kane, *Phys. Rev. Lett.* **100**, 096407 (2008).
 - [27] M. Sato and Y. Ando, *Reports on Progress in Physics* **80**, 076501 (2017).
 - [28] B. B. Roy, R. Jaiswal, T. D. Stanescu, and S. Tewari, *Phys. Rev. B* **110**, 115436 (2024).
 - [29] A. Y. Kitaev, *Annals. Phys.* **303**, 2 (2003).
 - [30] C. Nayak, S. H. Simon, A. Stern, M. Freedman, and S. Das Sarma, *Rev. Mod. Phys.* **80**, 1083 (2008).
 - [31] J. D. Sau, R. M. Lutchyn, S. Tewari, and S. Das Sarma, *Phys. Rev. Lett.* **104**, 040502 (2010).
 - [32] J. Sau and S. Tewari, in *Semiconductors and Semimetals*, Vol. 108 (Elsevier, 2021) pp. 125–194.
 - [33] A. D. Dolgov, *Surveys in High Energy Physics* **13**, 83 (1998), <https://doi.org/10.1080/01422419808240874>.
 - [34] J. Schober, I. Rogachevskii, and A. Brandenburg, *Phys. Rev. Lett.* **132**, 10.1103/physrevlett.132.065101 (2024).
 - [35] A. Vilenkin, *Phys. Rev. D* **22**, 3080 (1980).
 - [36] R. W. Jackiw, *Scholarpedia* **3**, 7302 (2008).
 - [37] I. Claude and Z. J. Bernard, Quantum field theory (1980).
 - [38] X. Huang, L. Zhao, Y. Long, P. Wang, D. Chen, Z. Yang, H. Liang, M. Xue, H. Weng, Z. Fang, et al., *Phys. Rev. X* **5**, 031023 (2015).
 - [39] Y. Wang, E. Liu, H. Liu, Y. Pan, L. Zhang, J. Zeng, Y. Fu, M. Wang, K. Xu, Z. Huang, et al., *Nat. Commun.* **7**, 13142 (2016).
 - [40] R. Dos Reis, M. Ajeesh, N. Kumar, F. Arnold, C. Shekhar, M. Naumann, M. Schmidt, M. Nicklas, and E. Hassinger, *New J. Phys.* **18**, 085006 (2016).
 - [41] F. Arnold, C. Shekhar, S.-C. Wu, Y. Sun, R. D. Dos Reis, N. Kumar, M. Naumann, M. O. Ajeesh, M. Schmidt, A. G. Grushin, et al., *Nat. Commun.* **7**, 11615 (2016).
 - [42] M. Wu, G. Zheng, W. Chu, Y. Liu, W. Gao, H. Zhang, J. Lu, Y. Han, J. Zhou, W. Ning, et al., *Phys. Rev. B* **98**, 161110 (2018).
 - [43] M.-X. Deng, G. Qi, R. Ma, R. Shen, R.-Q. Wang, L. Sheng, and D. Xing, *Phys. Rev. Lett.* **122**, 036601 (2019).
 - [44] H. B. Nielsen and M. Ninomiya, *Phys. Lett. B* **130**, 389 (1983).
 - [45] V. Aji, *Phys. Rev. B—Condensed Matter and Materials Physics* **85**, 241101 (2012).
 - [46] D. Son and B. Spivak, *Phys. Rev. B* **88**, 104412 (2013).
 - [47] S. Parameswaran, T. Grover, D. Abanin, D. Pesin, and A. Vishwanath, *Phys. Rev. X* **4**, 031035 (2014).
 - [48] A. Burkov, *Phys. Rev. B* **91**, 245157 (2015).
 - [49] N. Ong and S. Liang, *Nat. Rev. Phys.* **3**, 394 (2021).
 - [50] G. E. Volovik, *The universe in a helium droplet*, Vol. 117 (Oxford University Press on Demand, 2003).
 - [51] G. Xu, H. Weng, Z. Wang, X. Dai, and Z. Fang, *Phys. Rev. Lett.* **107**, 186806 (2011).
 - [52] A. Zyuzin, S. Wu, and A. Burkov, *Phys. Rev. B* **85**, 165110 (2012).
 - [53] P. Goswami and S. Tewari, *Phys. Rev. B* **88**, 245107 (2013).
 - [54] P. Goswami, J. Pixley, and S. D. Sarma, *Phys. Rev. B* **92**, 075205 (2015).
 - [55] S. Zhong, J. Orenstein, and J. E. Moore, *Phys. Rev. Lett.* **115**, 117403 (2015).
 - [56] K.-S. Kim, H.-J. Kim, and M. Sasaki, *Phys. Rev. B* **89**, 195137 (2014).
 - [57] R. Lundgren, P. Laurell, and G. A. Fiete, *Phys. Rev. B* **90**, 165115 (2014).
 - [58] A. Cortijo, *Phys. Rev. B* **94**, 241105 (2016).
 - [59] V. A. Zyuzin, *Phys. Rev. B* **95**, 245128 (2017).
 - [60] A. Kundu, Z. B. Siu, H. Yang, and M. B. Jalil, *New J. Phys.* **22**, 083081 (2020).

- [61] A. Knoll, C. Timm, and T. Meng, Phys. Rev. B **101**, 201402 (2020).
- [62] G. Bednik, K. Tikhonov, and S. Syzranov, Phys. Rev. Research **2**, 023124 (2020).
- [63] L. He, X. Hong, J. Dong, J. Pan, Z. Zhang, J. Zhang, and S. Li, Phys. Rev. Lett. **113**, 246402 (2014).
- [64] T. Liang, Q. Gibson, M. N. Ali, M. Liu, R. J. Cava, and N. P. Ong, Nat. Mater. **14**, 280 (2015).
- [65] C.-L. Zhang, S.-Y. Xu, I. Belopolski, Z. Yuan, Z. Lin, B. Tong, G. Bian, N. Alidoust, C.-C. Lee, S.-M. Huang, *et al.*, Nat. Commun. **7**, 1 (2016).
- [66] Q. Li, D. E. Kharzeev, C. Zhang, Y. Huang, I. Pletikosić, A. Fedorov, R. Zhong, J. Schneeloch, G. Gu, and T. Valla, Nat. Phys. **12**, 550 (2016).
- [67] J. Xiong, S. K. Kushwaha, T. Liang, J. W. Krizan, M. Hirschberger, W. Wang, R. J. Cava, and N. P. Ong, Science **350**, 413 (2015).
- [68] M. Hirschberger, S. Kushwaha, Z. Wang, Q. Gibson, S. Liang, C. A. Belvin, B. A. Bernevig, R. J. Cava, and N. P. Ong, Nat. Mater. **15**, 1161 (2016).
- [69] G. Sharma and S. Tewari, Phys. Rev. B **100**, 195113 (2019).
- [70] M. Wang, Q. Ma, S. Liu, R.-Y. Zhang, L. Zhang, M. Ke, Z. Liu, and C. T. Chan, Nat. Commun. **13**, 5916 (2022).
- [71] R. Arouca, A. Cappelli, and H. Hansson, SciPost Physics Lecture Notes [10.21468/scipostphyslectnotes.62](https://doi.org/10.21468/scipostphyslectnotes.62) (2022).
- [72] P. K. Tanwar, M. Ahmad, M. S. Alam, X. Yao, F. Tafti, and M. Matusiak, Phys. Rev. B **108**, L161106 (2023).
- [73] N. P. Ong and S. Liang, Nat. Rev. Phys. **3**, 394–404 (2021).
- [74] Q. Li and D. E. Kharzeev, Nucl. Phys. A **956**, 107 (2016), the XXV International Conference on Ultrarelativistic Nucleus-Nucleus Collisions: Quark Matter 2015.
- [75] S. Nandy, G. Sharma, A. Taraphder, and S. Tewari, Phys. Rev. Letters **119**, 176804 (2017).
- [76] G. Sharma, P. Goswami, and S. Tewari, Phys. Rev. B **93**, 035116 (2016).
- [77] G. Sharma, C. Moore, S. Saha, and S. Tewari, Phys. Rev. B **96**, 195119 (2017).
- [78] G. Sharma, S. Nandy, K. V. Raman, and S. Tewari, Phys. Rev. B **107**, 115161 (2023).
- [79] A. Ahmad and G. Sharma, Phys. Rev. B **103**, 115146 (2021).
- [80] A. Ahmad, K. V. Raman, S. Tewari, and G. Sharma, Phys. Rev. B **107**, 144206 (2023).
- [81] K. Das, S. K. Singh, and A. Agarwal, Phys. Rev. Res. **2**, 033511 (2020).
- [82] G. Sharma, P. Goswami, and S. Tewari, Phys. Rev. B **96**, 045112 (2017).
- [83] G. Sharma, S. Nandy, and S. Tewari, Phys. Rev. B **102**, 205107 (2020).
- [84] P. Goswami, G. Sharma, and S. Tewari, Phys. Rev. B **92**, 161110 (2015).
- [85] K. Das and A. Agarwal, Phys. Rev. Res. **2**, 013088 (2020).
- [86] A. Ahmad, G. Varma, and G. Sharma, Journal of Physics: Condensed Matter **37**, 043001 (2024).
- [87] A. Ahmad, G. V. K., and G. Sharma, Phys. Rev. B **111**, 035138 (2025).
- [88] X. Huang, L. Zhao, Y. Long, P. Wang, D. Chen, Z. Yang, H. Liang, M. Xue, H. Weng, Z. Fang, X. Dai, and G. Chen, Phys. Rev. X **5**, 031023 (2015).
- [89] L.-L. Gao and X.-G. Huang, Chin. Phys. Lett. **39**, 021101 (2022).
- [90] S. Cheon, G. Y. Cho, K.-S. Kim, and H.-W. Lee, Phys. Rev. B **105**, L180303 (2022).
- [91] S. Das, K. Das, and A. Agarwal, Phys. Rev. B **108**, 045405 (2023).
- [92] G. Varma, A. Ahmad, S. Tewari, and G. Sharma, Phys. Rev. B **109**, 165114 (2024).
- [93] A. Ahmad, G. V. K., and G. Sharma, Nonlinear anomalous hall effect in three-dimensional chiral fermions (2024), arXiv:2409.02985 [cond-mat.mes-hall].
- [94] H. Nielsen and M. Ninomiya, Phys. Lett. B **105**, 219 (1981).
- [95] H. Nielsen and M. Ninomiya, Phys. Lett. B **130**, 389 (1983).
- [96] N. Ashcroft, Thomson Learning **39** (1976).
- [97] S. de Groot and P. Mazur, *Non-equilibrium Thermodynamics*, Dover Books on Physics (Dover Publications, 1984).
- [98] R. J. DiPerna and P. L. Lions, Annals of Mathematics **130**, 321 (1989).
- [99] S. M. Girvin and K. Yang, *Modern Condensed Matter Physics* (Cambridge University Press, 2019).
- [100] C. Zeng, S. Nandy, and S. Tewari, Phys. Rev. Res. **2**, 032066 (2020).
- [101] C. Zeng, S. Nandy, and S. Tewari, Phys. Rev. B **105**, 125131 (2022).
- [102] D. Xiao, M.-C. Chang, and Q. Niu, Rev. Mod. Phys. **82**, 1959 (2010).
- [103] R.-H. Li, O. G. Heinonen, A. A. Burkov, and S. S.-L. Zhang, Phys. Rev. B **103**, 045105 (2021).
- [104] S. Nandy, C. Zeng, and S. Tewari, Phys. Rev. B **104**, 205124 (2021).
- [105] W.-Y. He, X. Y. Xu, and K. T. Law, Commun. Phys. **4**, 10.1038/s42005-021-00564-w (2021).
- [106] J. Kang and J. Zang, Phys. Rev. B **91**, 134401 (2015).
- [107] K. V. Samokhin, Phys. Rev. B **78**, 144511 (2008).